First-principles calculations of the band gap and optical properties of germanium sulfide

L. Makinistian[1,*] and E. A. Albanesi[1,2]
[1]*Facultad de Ingeniería, Universidad Nacional de Entre Ríos, 3101 Oro Verde (ER), Argentina*
[2]*INTEC-CONICET, Güemes 3450, 3000 Santa Fe, Argentina*
(Received 14 March 2006; revised manuscript received 16 May 2006; published 13 July 2006)

There are controversial results among the available experimental data of the germanium sulfide band gap, as well as between these results and the theoretical model-based band calculations published to date. To elucidate this situation, we performed an *ab initio* calculation of its electronic structure adopting the local density and generalized gradient approximations for the exchange-correlation potential. In addition, these calculations were carried out with and without the inclusion of the spin-orbit interaction. The main difference between our calculations and previous experimental and theoretical results is that we found several critical points in the valence and conduction bands that compete in defining the gap. This explains the diversity of the existent experimental results, which is also a consequence of the strong crystal anisotropy. Also, we suggest the important role of the *s*-Ge states contribution at the edge of the valence band. Based on our electronic structure, we discuss the experimental core spectra and optical properties of germanium sulfide. We found an excellent agreement between our results and the available experimental core spectra data. Furthermore, our calculated optical functions of GeS were satisfactorily compared against existing experimental data and they explain the origin of the optical transitions.

DOI: 10.1103/PhysRevB.74.045206 PACS number(s): 71.20.−b, 78.20.Ci, 71.15.Mb

I. INTRODUCTION

The IV-VI compounds have interesting electronic and optical properties. As to their technological application, they are used as cutoff devices and photovoltaic cells, and in the manufacture of infrared lasers[1–3] and detectors. They have also been studied for the evaluation of nanostructure etching.[4] Among these compounds, the rocksalt structured ones have been extensively studied, while the calchogenides of this family with a distorted structure (the black phosphorus structured GeS, GeSe, SnSe, and SnS) have been less thoroughly assessed.

Concerning GeS, several experimental studies have been performed, such as photoemission,[5] high resolution electron energy loss (HREELS),[6] reflectivity and transmittance,[7–9] Raman scattering,[9,10] photoelectron partial-yield and constant-initial-state (CIS) spectra,[11] and x-ray powder diffraction (for vibrational and structural analysis);[12] while only few theoretical calculations have been performed with the empirical pseudopotential method (EPM)[13] and with the linear combination of atomic orbitals method (LCAO).[14] Since we have found controversial results in the available literature, an exhaustive and updated theoretical study of GeS electronic and optical properties was needed.

GeS (along with GeSe, SnSe, and SnS) has an orthorhombic structure and belongs to the *Pnma* 62 (D_{2h}^{16}) space group. This material crystallizes in double layers that are perpendicular to the direction of the largest axis of the unit cell. The unit cell contains eight atoms organized in two adjacent double layers. The atoms in each double layer bond to their three nearest neighbors by covalent bonds of 2.441 Å and form a zigzag chain along the direction of the minor axis of the crystal (Fig. 1). The lattice parameters are $a=10.470$ Å, $b=3.641$ Å, and $c=4.297$ Å, corresponding to the $\Gamma\rightarrow X$, $\Gamma\rightarrow Y$, and $\Gamma\rightarrow Z$ directions in the first Brillouin zone (BZ), respectively (Fig. 2). Because of the dominant van der Waals character of the bonds between adjacent layers, this material cleaves easily along the *b*-*c* [100] planes. GeS (as the other three orthorhombic IV-VI compounds) has an intermediate behavior between a two-dimensional (2D) and a three-dimensional (3D) material.

In this paper, we present a thorough theoretical study of GeS based on *ab initio* calculations of its band structure, density of states (DOS), and optical properties. We discuss the location and nature (direct or indirect) of the band gap on the basis of our analysis of the crystal anisotropy, providing a unified discussion on these subjects which have been assessed in previous theoretical and experimental publications.

II. CALCULATION METHOD

We modeled GeS using a full potential linearized augmented plane waves (FP-LAPW) method,[15–21] within the

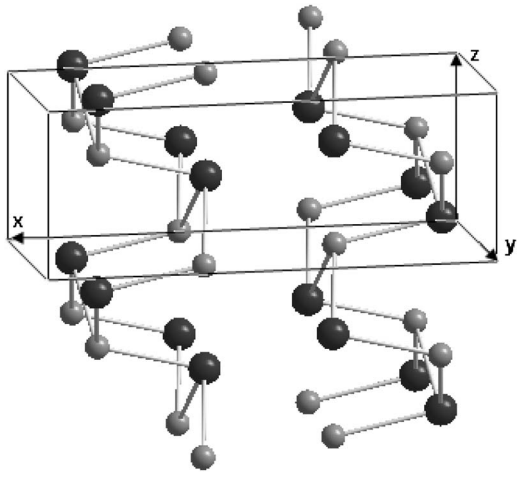

FIG. 1. The *Pnma* 62 orthorhombic structure of GeS.

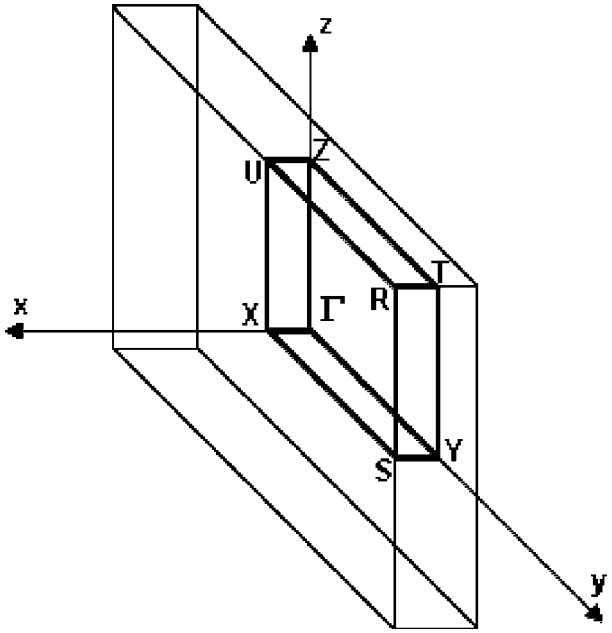

FIG. 2. The Brillouin zone, with axes x, y, and z corresponding to the crystal axes a, b, and c, respectively.

density functional theory (DFT).[22–24] For our calculations we used the WIEN2k packages,[25] which self-consistently finds the eigenvalues and eigenfunctions of the Kohn-Sham[26] equations for the system, using a R_{MT} of 2.29 (for both Ge and S), an l_{max} of 10 and a $R_{MT} \cdot K_{max}$ product of 7 (implying a plane wave expansion cutoff of ~9.31 Ry). As part of our approach, we used the local density approximation (LDA), in the Perdew-Wang parametrization,[27] for the exchange and correlation potential. This approximation has had great success in dealing with the calculation of electronic properties, although, as it is well known, it does not accurately describe some important properties (e.g., band gap underestimation). A formal correction is obtained when the gradient of the charge density is also considered. This is the so called generalized gradient approximation (GGA),[27,28] which we used in the formal parametrization scheme of Perdew-Burke-Ernzerhof (PBE).[29–31] This corrected functional is semilocal and thus more sensitive to nonspherical components of the density, which could result in a better performance when applied in a full potential scheme like the one implemented in WIEN2k. In spite of this general behavior of both approximations, and taking the GGA results as reference, we found that the LDA errors on the band gap and the band structure determination were remarkably small for GeS.

It is to be emphasized, though, that both LDA and GGA always yield underestimated band gaps, and that a usual empirical correction for this is the scissors operator,[32] which basically means to adjust the band gap with a constant potential to reproduce the experimental energy band gaps. This operator is often used, particularly in the determination of the band gap offsets[33,34] which appear when interfaces between different semiconductors are considered, and also when optical transitions are studied.[35] We used it in the optical spectra discussion in order to perform a detailed analysis of the optical transitions in GeS.

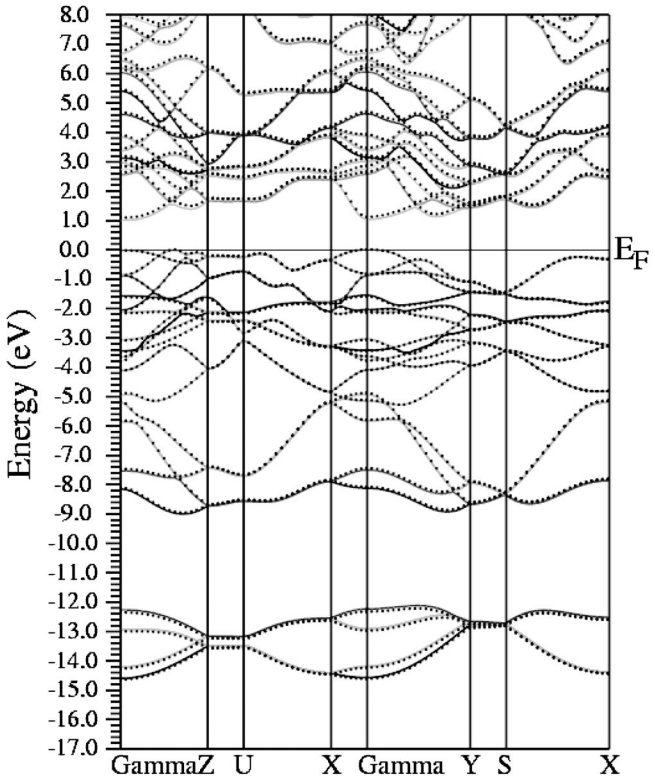

FIG. 3. Band structure with LDA (lines) and GGA (dots), both without the spin-orbit interaction.

III. BAND STRUCTURE AND DOS DISCUSSION

As shown in Fig. 3, there is no sensible difference between the band structures predicted by LDA and GGA approaches. As to the spin orbit, we found no important differences introduced by this interaction in both approximations, as can be seen by comparing the dotted and lined band structures shown for the GGA scheme in Fig. 4.

The main features of the electronic structure can be followed in Figs. 3–5. Between −14.61 and −12.13 eV a group of bands mainly corresponding to the 3s-S level can be seen. A bundle of bands originated from the 4s-Ge level and a slight contribution of the 3p-S level can be seen between −8.96 and −5.37 eV. These are followed by a group of bands formed by the hybridization of the 4p-Ge and 3p-S levels with a contribution of the 4s-Ge level toward the less binding energies, at the region closer to the Fermi energy (E_F), which extends from −5.37 eV up to 0 eV. With regard to the conduction band, it results from the hybridization of 4p-Ge and 3p-S, with minor contributions of 4s-Ge atomic orbitals (toward the least excited states) and of 4d levels of Ge and S from 6.30 eV up, approximately. Several degrees of degeneracy are observed depending on which of the different directions in the first BZ is under study: in the $\Gamma \rightarrow Z$, $X \rightarrow \Gamma$, and $\Gamma \rightarrow Y$ directions, 20 nondegenerated bands, except for the spin, are filled with the 40 valence electrons (16 corresponding to the Ge and 24 to the S); the $Z \rightarrow U$, $U \rightarrow X$, and $Y \rightarrow S$ directions present 10 bands with double degeneracy; and the S point (at the edge of the BZ) shows five values of energies with a fourfold degeneracy. The bands over the

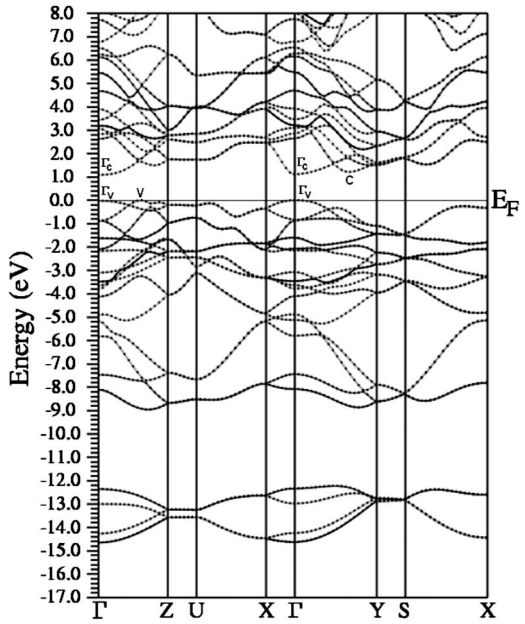

FIG. 4. Band structure with GGA, with (lines) and without (dots) the spin-orbit interaction. The critical points that could compete for the definition of the gap are labeled.

$\Gamma \rightarrow X$ line (corresponding to the largest lattice parameter, i.e., to the axis perpendicular to the cleavage plane of the crystal) indicate a strong decrease of the mobility of the charge carriers for the lowest energies of the conduction band and the highest of the valence band, in concordance with the strong anisotropy of the system in that direction.

The total and partial (s, p, and d atomic orbitals) densities of states obtained in this work are shown in Fig. 5. It can be seen that they are in agreement with the afore mentioned description of the band structure, which presents three well defined regions below the Fermi energy. Also, in this figure, our total DOS calculated with the GGA is compared against experimental curves obtained with photoemission measurements[5,11] and against the result of the only previous DOS calculations, obtained with the linear combination of atomic orbitals (LCAO) method.[14] When comparing DOS curves, it is usual to take the top of the valence band as a reference of zero. However, one of the difficulties encountered in photoemission measurements is to determine reference energies precisely, since the broadening tails going through zero appear not to be very well defined. Thus, to avoid this problem, we have chosen to align the sharp edge closer to the Fermi level corresponding to the s cation orbital. As regards the locations of the main structures of the DOS, ours correlate very satisfactorily with those of the experimental curves.

The DOS calculated with the LCAO method shows differences with the other curves both in the energy positions and in the valence bandwidths. This is mainly due to the fact that the LCAO calculation was implemented with only nearest neighbor interactions. A drawback of this implementation is that it does not offer a good hybridization description. As a consequence, the bands and DOS appear quite decoupled (i.e., there is less overlapping among the different contributions than in our calculations), thus the material layered structure is exaggerated.

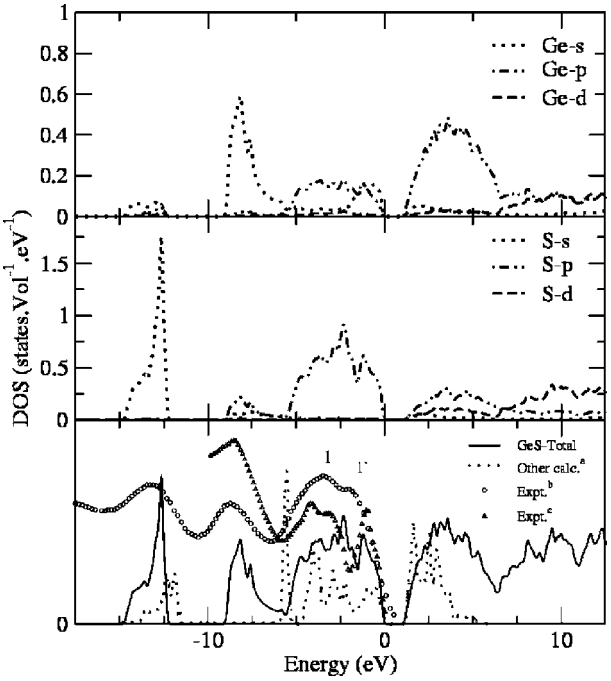

FIG. 5. DOS of the s, p, and d orbitals of the Ge and the S. Total density: our calculation, other authors' calculation [a]Ref. 14 and an experimental result, [b]Ref. 5.

The enhanced description of hybridization that our calculations perform has important consequences: our band structure and DOS differ from the ones published to date in different directions of the BZ. These differences appear mainly in the lower and upper regions of the conduction and valence bands, respectively. This fact affects the nature and location of the band gap, that has been contradictorily reported: direct from EPM results,[13] but indirect with the LCAO method,[14] located in both cases at approximately $\frac{3}{4}$ from Γ, in the $\Gamma \rightarrow Z$ direction. To stress this point, we wish to highlight that in Fig. 4 the directions involving the Γ point, which is the most symmetrical region in the BZ, are the most hybridized. Thus, those are the regions where the spreading and crossing of bands are increased. The $Z \rightarrow U$ and $Y \rightarrow S$ directions are, instead, less symmetrical and hybridization decreases. In Fig. 6 we plot the band structure in planes $R \rightarrow U \rightarrow Z \rightarrow T$ and $R \rightarrow S \rightarrow Y \rightarrow T$, showing that the material becomes rather decoupled (i.e., less hybridized) only in these special regions, obtaining the most decoupled bands for the least symmetrical direction, which is the $R \rightarrow S$ edge. The material as a whole, however, maintains hybridization as an important key to building those physical properties mainly determined by the morphology of the top and bottom parts of the valence and conduction bands, respectively.

As can be seen in Fig. 5, an important feature about the whole valence band closer to E_F (from −5.37 to 0 eV) is that the experimental curve reported in Ref. 5 for this region shows a structure of double peaks called 1 and 1′. These were postulated as a striking p-states feature, also appearing in the DOS measured in Ref. 11. Our calculated curve for this region adjusts very well to this double peak structure, showing that an important s-cation states contribution is present in peak 1′. The details of our results show that this

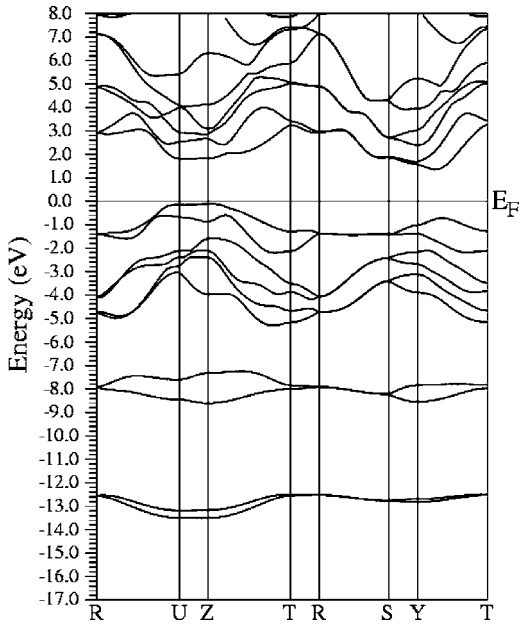

FIG. 6. Our *ab initio* calculated band structure, with GGA and including spin-orbit interaction, in less symmetrical directions in the BZ.

region is typically a p-band type formed mostly by the hybridization of the stronger $3p$-S levels with the $4p$-Ge, and the narrower $4s$-Ge levels at the edge of the valence bands, which strongly contribute to the valence band maximum (VBM) formation. We postulate the presence of these s-cation states, hybridized with the p-cation and p-anion contributions, as the most important feature in defining most physical properties, since they shape the behavior of the maxima that determine the band gap. This had already been found to be the key to band gap formation in cubic IV-VI compounds,[36–38] and consequently in the physical properties of those materials. The resemblance between the physical properties of orthorhombic[5,11] IV-VI materials among themselves has also been well established. So far, and still being aware of the differences between cubic and orthorhombic IV-VI compounds, we suggest this behavior of the s-cation states at the edge of the valence band is the fingerprint of the IV-VI compounds. Hence all descriptions should account for it in order to explain the physical properties of this family of compounds.

In order to facilitate the following discussions, in Table I we present the composition of the peaks v_1 through v_6 in the valence bands of the DOS as they are shown in Fig. 7, in terms of states type, and the kind of atom from which they are originated. In the table we have also included the same information about the main peaks of the conduction bands DOS, named A-B, A'-B', c_1 and c_2.

A. Location of the energy band gap

With regard to the energy band gap, our calculations showed several energy gaps that compete for its definition (Fig. 4). On one hand, the valence band presents two competing maxima: one at Γ, named Γ_V in Fig. 4, and the other at approximately $\frac{1}{2}$ from Γ, in the $\Gamma \rightarrow Z$ direction, named V, only 0.016 eV above Γ_V. On the other hand, there are two minima in the conduction band that could define the energy gap, named Γ_C and C in Fig. 4. In particular, C is located at $\frac{2}{3}$ from Γ, in the $\Gamma \rightarrow Y$ direction and only 0.09 eV above Γ_C. Thus, in addition to the direct transition of 1.12 eV that occurs at the Γ point ($\Gamma_V \rightarrow \Gamma_C$ at the center of the BZ), two more, indirect transitions of almost the same amplitude in energy are to be considered: (a) $V \rightarrow \Gamma_C$, of 1.10 eV; and (b)

TABLE I. Relevant calculated DOS peaks and their contributing states. To facilitate further discussions on the optical transitions, we have corrected the band gap with the scissors operator.

		Contributing states	
DOS peak	DOS energy	Main	Minor
v_6	−4.73	p-S	p-Ge
v_5	−2.81	p-S	p_z-Ge
v_4	−2.32	p_z, p_x, p_y-S	p-Ge
v_3	−1.85	p_z-S	p-Ge
v_2	−1.22	p_y-S	p_y-Ge
v_1	−0.52	p-S, s-Ge	
VBM	0	s-Ge, p_x, p_y-S	p_z-S
A-B	2.56	p_z, p_x-Ge	p-S
A'-B'	2.83	p_x-Ge	p-S
c_1	3.33	p_x-Ge	p-S
c_2	5.84	p_y-Ge	p_y, p_z-S

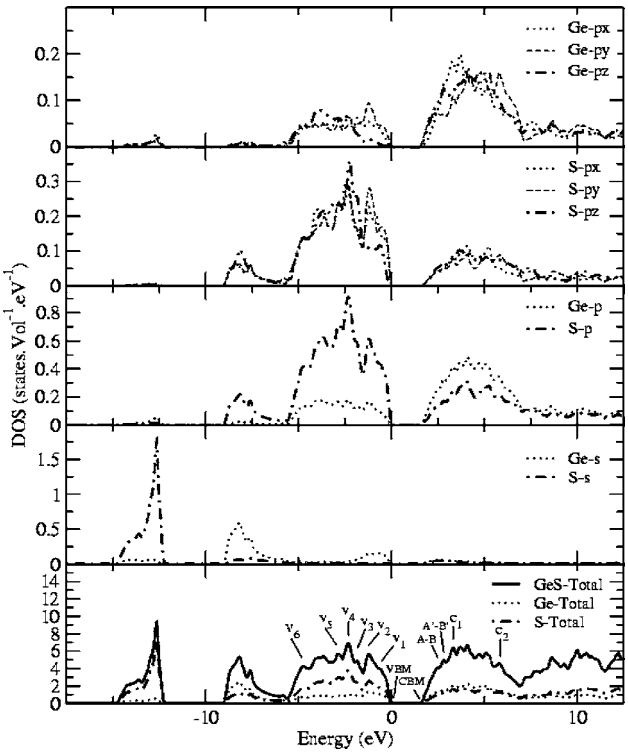

FIG. 7. Density of the states of the p_x, p_y, and p_z orbitals of the Ge and the S. To facilitate further discussion on the optical transitions, we have corrected the band gap with the scissors operator.

TABLE II. Experimental and theoretical values of the GeS energy band gap. Values are in eV.

Experimental	Theoretical	
	Our calculations	Others' calculations
1.65 direct in $\Gamma \rightarrow Z$[a]		
1.65 direct allowed in the $\Gamma \rightarrow Z$[b]		
1.540 indirect in $\Gamma \rightarrow Z$[c]	1.10 indirect in $\Gamma \rightarrow Z$ (V to Γ_c)	Only 1.52 indirect in $\Gamma \rightarrow Z$[d] at $\frac{3}{4}$ from Γ
1.5 (electrical energy gap)[c]		
1.58 (electrical energy gap)[c]	1.12 direct on the Γ point	
1.56 allowed indirect both in $\Gamma \rightarrow X$ and $\Gamma \rightarrow Z$[c]		
1.65 allowed direct in $\Gamma \rightarrow Z$ and nonconclusive with respect to $\Gamma \rightarrow X$[b]		Only 1.2±0.2 direct in $\Gamma \rightarrow Z$[e] at $\frac{3}{4}$ from Γ
1.56 indirect, the same for $\Gamma \rightarrow Z$ and $\Gamma \rightarrow X$[c]	1.28 indirect in $\Gamma \rightarrow Y$ (Γ to C)	
1.35 and 1.50 (photoconductivity energy gap)[c]		
2.04 in $\Gamma \rightarrow Z$ and 1.8 in $\Gamma \rightarrow Y$ (both direct conductivity gaps)[f]		
1.613±0.010 in $\Gamma \rightarrow Z$ (photoconductivity energy gap)[g]		

[a]Reference 7.
[b]Reference 42.
[c]Reference 8.
[d]Reference 14.
[e]Reference 13.
[f]Reference 43.
[g]Reference 44.

$\Gamma_V \rightarrow C$, of 1.21 eV. All these values were obtained without using the scissors operator. As to the DOS calculated to discriminate the contribution of the different p orbitals (p_x, p_y, and p_z) (Fig. 7), it indicates a higher probability of transitions from the p_x and p_y levels than from the p_z levels. But these orbitals are the main contributors to both Γ_V and V. Thus, this fact supports the hypothesis that both maxima compete for the definition of the gap (even though a direct transition can occur without the energy of a phonon) without suggesting, however, a preference of the system for either of them.

While the available data from angular resolved photoemission spectrometry (ARPES) measurements[13] indicate a direct gap of 1.20 eV in the $\Gamma \rightarrow Z$ direction, in reflectivity and transmittance experiments, Elkorashy[8] found a 1.540 eV indirect gap in the $\Gamma \rightarrow Z$ direction. This indirect gap is followed by another, in the $\Gamma \rightarrow X$ direction, slightly greater by an order of 10^{-2} eV. In absorption coefficient measurements,[8] two possible gaps were obtained, both indirect and of 1.56 eV, but one in the $\Gamma \rightarrow Z$ direction and the other in the $\Gamma \rightarrow X$ one. This diversity of apparently contradictory experimental results can be explained by our findings. They show the existence of different possible gaps (direct and indirect), very close in energy and in different locations of the BZ. These gap measurements might depend on the conditions in which the experiment is carried out. In particular, those experiments that are not performed at low enough temperatures allow the occurrence of indirect transitions through phonons. Also, the anisotropy of the crystal makes its contribution to determine the results, which strongly depend on the crystallographic directions considered in each experiment. Table II shows a summary of our possible band gaps and others found in the literature (experimental and theoretical). Figure 8 allows one to compare our band structure to that of Ref. 13, where two main features can be noticed.

First, although there is an overall agreement concerning the bands' morphology, the EPM bands seem to be stretched downward (not rigidly shifted downward). This is clear from paying attention to the $\Gamma \rightarrow Z$ direction: in spite of coinciding at the Fermi level, EPM bands go down to more negative energies than ours. This fact is particularly evident concern-

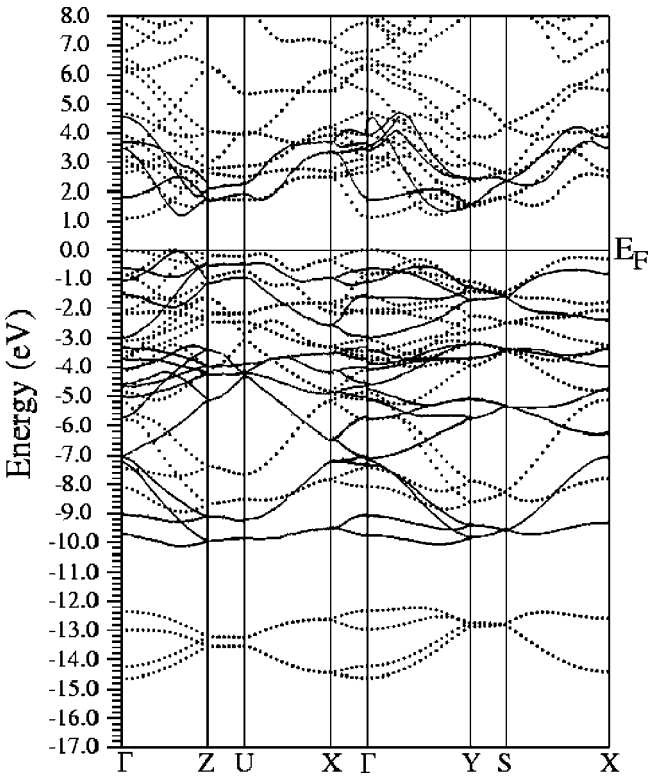

FIG. 8. Our *ab initio* calculated band structure (dots) overlaid upon the EPM calculated bands of Ref. 13.

ing the bundle corresponding to the 3*s*-S states, which our calculations locate at about 13.30 eV, while EPM locates at about 19.50 eV, not shown in Fig. 8. Secondly, while in the EPM bands a direct band gap on the $\Gamma \rightarrow Z$ line is found (and no other to compete), in our bands the different possible competing band gaps discussed previously are displayed. The fact that the experimental densities of states presented in Fig. 5 agree with our results, supports them as the correct ones.

B. Core excitation spectra

Taniguchi *et al.*[11] have measured the partial-yield spectra of GeS, which is representative of the absorption spectrum in the core excitation region for the electric field component parallel to *c* (called *a* in their paper) and *b* axes, $\vec{E} \| c$ and $\vec{E} \| b$, respectively. It represents the interaction of the 3*d*-Ge core levels (cation spectra) and the 2*p*-S core levels (anion spectra) with the conduction bands.

C. Cation spectra

We can use the experimental values for both the band gap and the measured Ge $3d_{5/2}$ and Ge $3d_{3/2}$ multiplets to explain the core absorption spectrum through interaction with the conduction band. The experimental values[11] from core-level photoemission measurement added to the experimental band gap energy give 31.10 and 31.63 eV for the Ge $3d_{5/2}$ and the Ge $3d_{3/2}$ states, respectively. These energies account for the transition to the bottom of the conduction band, namely, the conduction band minimum (CBM). Taniguchi *et al.*[11] found these two main peaks, each of them with a double structure. The first double structure corresponds to the Ge $3d_{5/2}$ and its two peaks, called A and B, occur at 30.83 and 31.05 eV for $\vec{E} \| c$, and at 30.83 and 31.01 eV for $\vec{E} \| b$, respectively. The second double structure corresponds to the Ge $3d_{3/2}$, with its two peaks called A' and B', located at 31.47 and 31.68 eV for $\vec{E} \| c$, and at 31.45 and 31.65 eV for $\vec{E} \| b$, respectively. Using the existing theoretical calculations,[13] they suggested this structure be produced by a first conduction band doublet of rather parallel bands splitted by about 0.3 eV, located in the $Z \rightarrow U$ direction of the BZ, which appear about 0.5 eV above the CBM.

Our band structure does not show such double bands in one preferential direction in the BZ. However, we can explain the *A*-*B* and A'-B' structures, as originated from a cooperative effect produced by rather flat bands appearing in different regions in the BZ. The first structure, *A*-*B*, shown in our DOS conduction band in Fig. 7, comes mainly from the first single, flat, conduction bands in the directions $Z \rightarrow U$, first $\frac{1}{3}$ of $U \rightarrow X$, $Y \rightarrow S$, first $\frac{1}{2}$ of $S \rightarrow X$, and first $\frac{1}{3}$ of $Y \rightarrow T$, together with the rest of the mixed bands about that energy in the whole BZ. The second structure, A'-B', comes mainly from the first, flat conduction bands in the directions $Z \rightarrow U$, last $\frac{1}{3}$ of $U \rightarrow X$, $X \rightarrow \Gamma$, $Y \rightarrow S$, and last $\frac{1}{3}$ of $S \rightarrow X$. All mentioned contributions, together with the rest of the bands mixed round each energy in the whole BZ, give the well resolved peaks shown as *A*-*B* and A'-B' in our conduction band DOS (Fig. 7). The first peak has a flat upper region which extends from about 0.88 up to 0.96 eV above the CBM, while the second peak is well defined at 1.16 above CBM. These peaks are responsible for our theoretical fine structure *A*-*B* and A'-B' splitting, both in the range from 0.20 to 0.28 eV, compared to the 0.18 and 0.20 eV, respectively, for the experimental $\vec{E} \| c$ measurement; and the 0.22 and 0.21 eV, respectively, for the experimental $\vec{E} \| b$ measurement. For comparison, our theoretical results without the spin-orbit interaction yield the *A*-*B* and A'-B' fine structure splitting range at about 0.25 to 0.30 eV in the Ge 3*d* core absorption spectrum, and the effect is produced in the same locations as when spin orbit is present.

D. Anion spectra

In GeS, the spin-orbit splitting of the 2*p*-S core level is about 1.2 eV.[11] Taniguchi *et al.*[11] have measured the partial-yield spectra for the *S* $2p_{3/2}$ and *S* $2p_{1/2}$ core doublet, for $\vec{E} \| c$, and $\vec{E} \| b$, obtaining two broad peaks at 162.9 and 164.2 eV, naming them *a* and a', respectively. They attribute this structure to the spin-orbit doublet, since both splitting energies are about the same. Their peak *a* appears about 0.7 eV above the core absorption threshold. Following the previous discussion for the cation core spectra, they assigned the structure to the transition to the first conduction band doublets, of rather parallel bands, in the $Z \rightarrow U$ and $Y \rightarrow S$ directions of the BZ.

In our calculation, the a-a' structure relies on the transition from the core $2p_{3/2}$ and *S* $2p_{1/2}$ levels to the *A*-*B* peak in the conduction band of the DOS. If together with these anion core transitions, we consider the same transition but from the main *p*-S peak in the valence band DOS, which is the v_2 peak in Fig. 7, we should obtain a strong contribution in our optical functions at about 3.78 eV, and that is actually the E_2 peak in ε_{2zz} at 3.71 eV (see Table V).

In the same way that LDA and GGA are known to underestimate the band gaps, they are also known to disagree in giving the 3*d* core levels by about 1–4 eV higher in energy than the experimental values. Furthermore, the description of the conduction band states could be improved,[39,40] since DFT is primarily a ground state formalism. At present, and still using the DFT framework as a starting point, some powerful techniques involving a two particle operator to describe the excitonic effect for the electron-hole pair are being implemented,[35,41] so as to consider excitons on the absorption spectra. Our estimations on the core excitation spectra, and the persistence of some experimental discrepancies[11] on the problem, suggest that a thorough study of the excitonic effect on GeS is worth undertaking. That study is under consideration at present.

IV. OPTICAL PROPERTIES

We have performed the calculation of the imaginary part of the complex dielectric function $\varepsilon_2(\omega)$ integrating in *k* space by the standard tetrahedron-method[45] and of the real part $\varepsilon_1(\omega)$ through the Kramers-Kronig relations. The expression of the imaginary dielectric functions is computed by Ambrosch-Draxl and Abt,[46] and the following is the general

expression for the imaginary part of the dielectric tensor:

$$\varepsilon_2(\omega)_{\alpha\beta} = \frac{4\pi^2 e^2}{m^2\omega^2}\sum_{i,f}\int \langle f|p_\alpha|i\rangle\langle i|p_\beta|f\rangle \times W_i(1-W_f)\delta(E_f - E_i - \hbar\omega)d^3k. \quad (1)$$

In this expression, $\langle f|p_\alpha|i\rangle$ and $\langle f|p_\beta|i\rangle$ are the dipole matrix elements corresponding to the α and β directions of the crystal (x, y or z), and f, i are the final and initial states, respectively. W_n is the Fermi distribution function for the nth state, and E_n is the electron energy in the nth state. The real part of the diagonal dielectric functions is computed from $\varepsilon_2(\omega)$ using the Kramers-Kronig relations in the form

$$\varepsilon_1(\omega)_{\alpha\alpha} = 1 + \frac{2}{\pi}P\int_0^\infty \frac{\omega'\varepsilon_2(\omega')_{\alpha\alpha}}{\omega'^2 - \omega^2}d\omega', \quad (2)$$

where P means the principal value of the integral. In order to achieve a comprehensive understanding of the optical behavior of the system, we first computed the complex dielectric function, and then calculated the real and imaginary parts of the complex refraction index $\tilde{n}(\omega)_{\alpha\alpha} = n_R(\omega)_{\alpha\alpha} + ik(\omega)_{\alpha\alpha}$, where $n_R(\omega)$ is the ordinary refraction index and $k(\omega)$ is the coefficient of extinction, obtained from $[\tilde{n}(\omega)_{\alpha\alpha}]^2 = \varepsilon_1(\omega)_{\alpha\alpha} + i\varepsilon_2(\omega)_{\alpha\alpha}$. Finally, we computed the coefficient of absorption $\alpha(\omega)$ as follows:

$$\alpha(\omega)_{\alpha\alpha} = \frac{2\omega}{c}\left(\frac{-\mathrm{Re}[\varepsilon(\omega)_{\alpha\alpha}] + |\varepsilon(\omega)_{\alpha\alpha}|}{2}\right)^{1/2} \quad (3)$$

and the reflectivity $R(\omega)$ as

$$R(\omega)_{\alpha\alpha} = \left|\frac{1-\tilde{n}(\omega)_{\alpha\alpha}}{1+\tilde{n}(\omega)_{\alpha\alpha}}\right|^2. \quad (4)$$

In order to improve the comparison with the experimental optical spectra, we performed our following optical calculations using the scissors operator (with a constant shift of 0.53 eV) as implemented in the WIEN2k optical package: a rigid shift of the imaginary part of the dielectric function is performed previous to the application of the Kramers-Kronig relations for the obtention of the real part of ε.

A. Convergence and spin-orbit influence

Since ε_2 is usually calculated first, we chose it as a reference for the assessment of convergence and the influence of the spin-orbit interaction on the optical properties. On one hand, Fig. 9 shows ε_2 with increasingly finer meshes for the discretization of the BZ. It is clearly seen that the 90 k-points calculation did not converge, while the 2646 and 4950 k-points calculations coincide. Thus, we assumed convergence at 2646 and this is the number of k points we used for the calculation of the optical properties. On the other hand, Fig. 10 confirms what was to be expected from the very small effect of the spin-orbit interaction on the band structure discussed above, namely, that it does not introduce practical differences in the optical properties either.

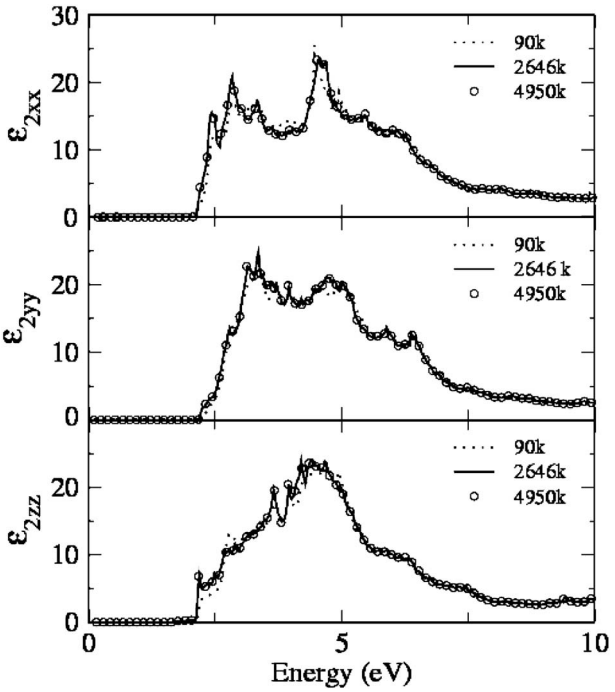

FIG. 9. Imaginary part of the complex dielectric function computed with 90, 2646, and 4950 k points in the BZ.

B. Scattering

Two closely related optical parameters indicate how electromagnetic energy is dispersed when it penetrates in a medium: the real part of the complex dielectric function (ε_1) and the real part of the complex refraction index (n). Figures 11 and 12 show these parameters for the three crystal axes: a, b, and c (xx, yy, and zz, respectively) and Tables III and IV list the characteristic values.

Corresponding to the largest axis, ε_{1xx} presents two sharp peaks (E_0 and E_2) at 1.88 and 3.84 eV and a negative valley

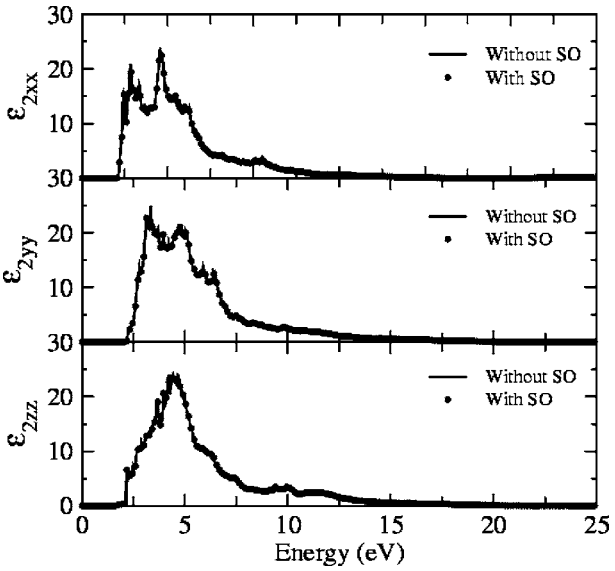

FIG. 10. Imaginary part of the complex dielectric function computed with and without the inclusion of the spin-orbit interaction.

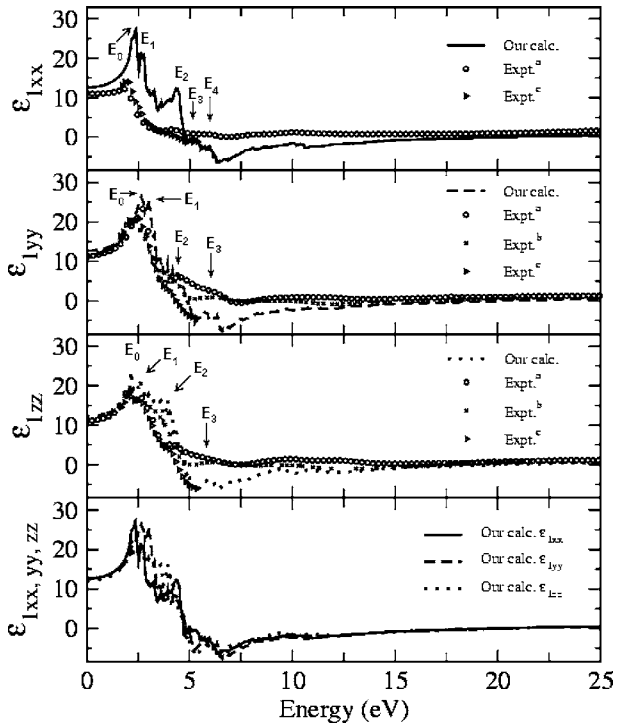

FIG. 11. Calculated and experimental real part of the dielectric function. [a]Ref. 47, [b]Ref. 7, [c]Ref. 48.

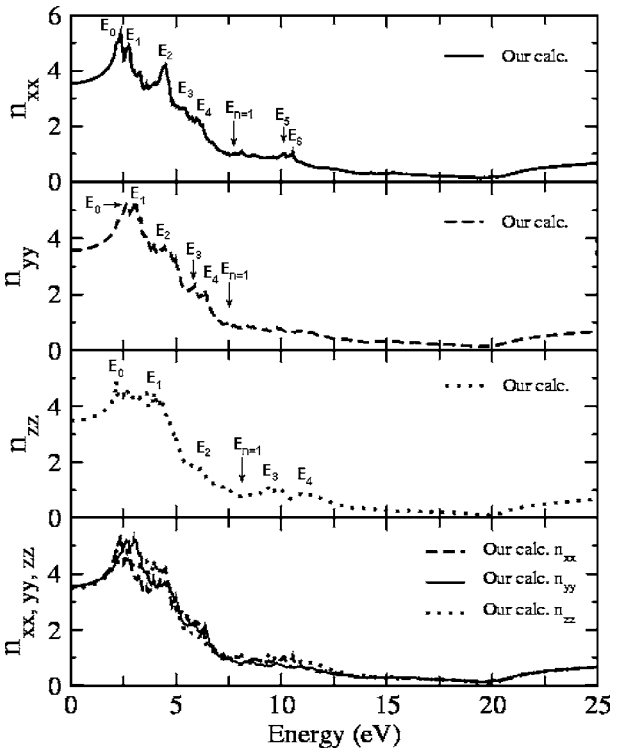

FIG. 12. Calculated real part of the complex index of refraction.

TABLE III. Real part of the complex dielectric function. All $\epsilon_1(0)$ are adimensional, while the energies E_i are in eV.

	ϵ_{1xx}		ϵ_{1yy}		ϵ_{zz}	
$\epsilon_1(0)$/peaks	Our calc.	Expt.	Our calc.	Expt.	Our calc.	Expt.
$\epsilon_1(0)$	12.18	10.44[a]	11.26	10.59[a]	11.47	10.28[a]
				10.59[b]		10.28[b]
		5.89[c]		8.89[c]		7.92[c]
		7.15[c]		6.91[c]		7.15[c]
		7.91[c]		10.48[c]		10.33[a]
		8.4[c]		10.01[c]		9.49[c]
						11.1[c]
E_0	2.40	1.92[a]	2.70	2.72[a]	2.17	
		2.078[c]		2.11[b]		
				2.047[c]		
E_1	2.68		3.04	2.610[c]	2.64	1.99[a]
						1.99[b]
						2.037[c]
E_2	4.34		4.24	4.57[a]	3.81	2.63[a]
				4.043[c]		2.63[b]
						2.637[c]
E_3	5.18		5.93	6.36[a]	5.90	4.19[a]
				6.05[b]		5.98[b]
E_4	5.85					

[a]Reference 47.
[b]Reference 7.
[c]Reference 48.

TABLE IV. Characteristic values and peaks of the real part of the complex index of refraction (n). All values are in eV, except for $n(0)$ which are adimensional.

	n_{xx}	n_{yy}	n_{zz}
$n(0)$	3.51	3.55	3.49
$E(n=1)$	7.78	7.41	7.47
E_0	2.39	2.67	2.11
E_1	2.76	2.97	4.05
E_2	4.51	4.42	6.18
E_3	5.32	5.87	9.66
E_4	6.00	6.39	11.26
E_5	10.12		
E_6	10.55		

at 5.88 eV. Both experimental curves[47,48] show a single rounded maximum which corresponds to our E_0-E_1 peaks, although neither of them show our fine structure peaks. The first peak of Ref. 47 is at the end of a rather flat structure that begins at zero energy, and does not show any other structure resembling our E_2-E_3 calculation, except for a weak increase at the position of our E_2 peak. The other experimental result[48] corresponds to measurements from 1.66 to 5.5 eV and meets our result at the end of its fall (E_3 and E_4). With respect to the b axis, ε_{1yy}, our calculations show a rounded peak with two sharper ones at its top (E_0 and E_1, at 2.11 and 2.44 eV, respectively). This rounded structure is in good correspondence with all the experimental curves up to E_2. Beyond this peak, two of the experimental curves[7,47] stop falling, going stationary about zero, but the experimental results of Ref. 48 still drop below zero in coincidence with our calculations in all the range of their measurements (up to E_3 at 5.50 eV). This situation also stands for the z axis. In this direction, ε_{1zz} presents a prominent peak (E_0) which is closely followed by another one (E_1), a flat shoulder and a third, sharper one (E_2). Our calculations satisfactorily agree with two of the experimental results up to about 4.00 eV, and agree with that of Logothetidis *et al.*[48] in the whole range of their measurements. With respect to the values at zero energy, our results show a low overestimation of the dielectric constant $\varepsilon(0)$ for the three axes (see Table III).

With regards to n, notable features [peaks, shoulders, the refraction index for zero energy $n(0)$, and the first energy for which dispersion is null $E(n=1)$] are extracted in Table IV. It is interesting to notice that in the range of about 7.50–10.00 eV, GeS shows almost no dispersion (i.e., $n \approx 1$) for the three axes, as shown in Fig. 12. For this same range of incident energy, a drop of the reflectivity is observed, as can be seen in Fig. 18.

C. Energy intake

The imaginary part of the dielectric function ε_2, and the coefficients of extinction k, absorption α, and reflectivity R, represent different ways to assess how the electromagnetic energy is taken when interacting with a material medium. In order to perform a comprehensive study of this important aspect of the optical properties of GeS, we have also computed and studied these parameters.

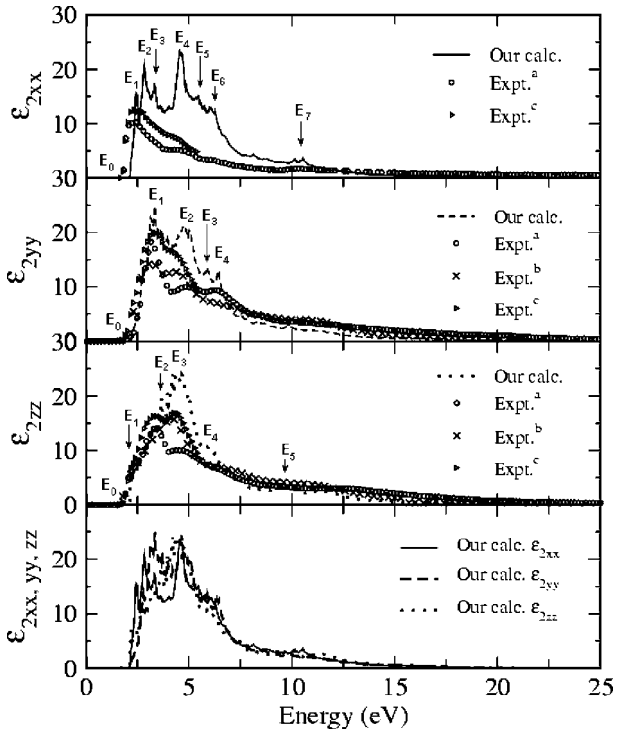

FIG. 13. Calculated and experimental imaginary part of the dielectric function. [a]Ref. 47, [b]Ref. 7, [c]Ref. 48.

Following our previous discussion in Sec. III, the deep valley around −1.60 eV in p_x-S and p_y-S DOS in Fig. 7 also seems to account for a similar morphology of ε_{2xx} and ε_{2yy} curves (Fig. 13) and, actually, for the rest of the optical spectra. As to the specific origin of peaks, in Figs. 14 and 15 we show our bands for two different paths on the BZ, with the arrows representing possible interband transitions, originating the main E_i peaks in the optical function spectra. From these and from Fig. 7, we find that ε_{2xx} peak E_1 originates between the VBM and b region in the CBM with 2.39 eV, while E_2 comes from the transition v_1 to the conduction band region A-B, which is mainly formed by p-Ge states. The valence band states are originated by the hybridized contribution of s-Ge and p_x, p_y -S at about the edge of the valence band. The peak E_1 in ε_{2zz} is also produced by the transition v_1 to A-B. Peak E_3 comes from the transition from v_1 region, the first valence band s-Ge and p_y-S contribution, but to the region A'-B' in the conduction band. This peak corresponds to the E_1 peak in ε_{2yy}, slightly modified by the material anisotropy. The most prominent peak in the optical spectra is E_4, mainly due to interband transitions from p_x, p_y-S states of the valence band in the v_3 region, to p_x-S and p_x-Ge states in the conduction band region A'-B'. This peak is clearly present in the three main crystallographic directions, since it corresponds to the slightly shifted peaks E_2, to higher energy, and E_3 to lower energy, in ε_{2yy} and ε_{2zz}, respectively. A similar situation occurs with the double peak E_6 occurring at 6.09 eV, coming from the $v_5 \rightarrow c_1$ transition. This peak corresponds to the structure E_3-E_4 in ε_{2yy}, and to the peak E_4 in ε_{2zz}. The double peak E_7 appears to be a consequence of

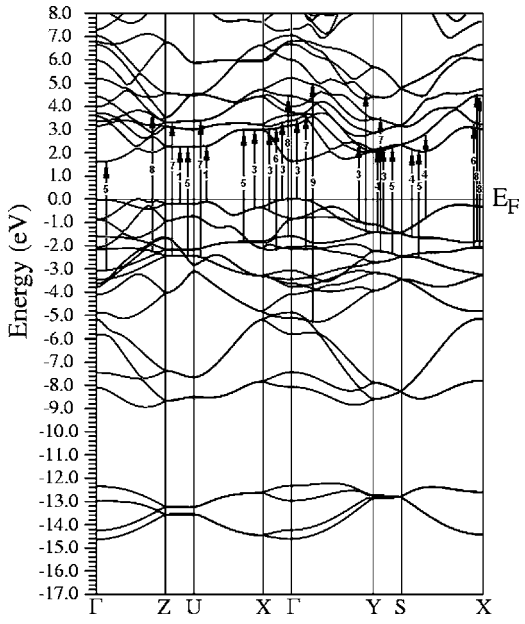

FIG. 14. Band structure for the most symmetrical directions in BZ, with the scissors operator applied. See Fig. 2. The arrows represent possible interband transitions between bands originating the main peaks in the optical function spectra.

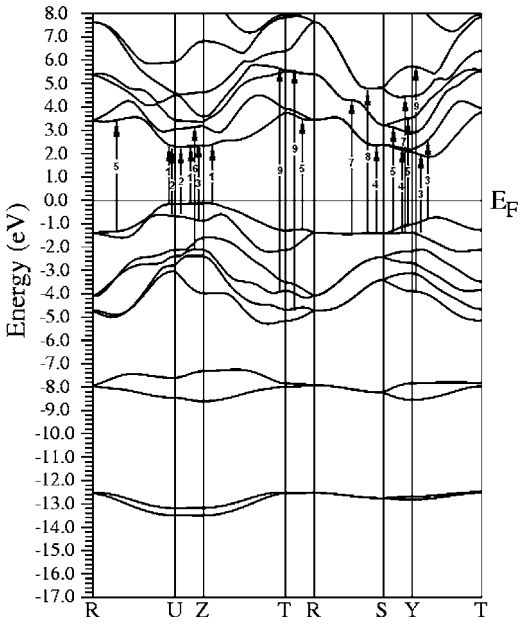

FIG. 15. Band structure for less symmetrical directions in BZ, with the scissors operator applied. See Fig. 2. The arrows represent possible interband transitions between bands originating the main peaks in the optical function spectra.

TABLE V. Imaginary part of the complex dielectric function. Energies are in eV. Numbers in the "bands" column correspond to the arrows in Figs. 14 and 15.

Transitions		ε_{2xx}			ε_{2yy}			ε_{2zz}		
DOS	Bands	Peak	Our calc.	Expt.	Peak	Our calc.	Expt.	Peak	Our calc.	Expt.
		E_0	2.08	1.85[a]	E_0	2.16	1.81[a]	E_0	2.16	1.84[a]
				1.85[c]			1.81[b]			1.84[b]
							1.81[c]			1.84[c]
$v_{VBM} \rightarrow A\text{-}B$	1	E_1	2.42					E_1	2.39	2.26[a]
										2.26[b]
										2.26[c]
$v_1 \rightarrow A\text{-}B$	2	E_2	2.82	2.31[a]						
				2.30[c]						
$v_1 \rightarrow A'\text{-}B'$	3	E_3	3.34	2.68[c]	E_1	3.40	3.17[a]			
							3.17[b]			
							3.33[c]			
$v_2 \rightarrow A\text{-}B$	4							E_2	3.71	3.47[a]
										3.39[b]
$v_3 \rightarrow A'\text{-}B'$	5	E_4	4.60	4.43[a]	E_2	4.76	4.85[a]	E_3	4.58	4.53[a]
				4.43[c]			4.49[b]			4.38[b]
							4.27[c]			4.38[c]
$v_5 \rightarrow A\text{-}B$	6	E_5	5.40							
$v_5 \rightarrow c_1$	7				E_3	5.87				
$v_5 \rightarrow c_1$	8	E_6	6.09	6.12[a]	E_4	6.39	6.40[a]	E_4	6.00	
$v_6 \rightarrow c_2$	9	E_7	10.27					E_5	9.65	

[a]Reference 47.
[b]Reference 7.
[c]Reference 48.

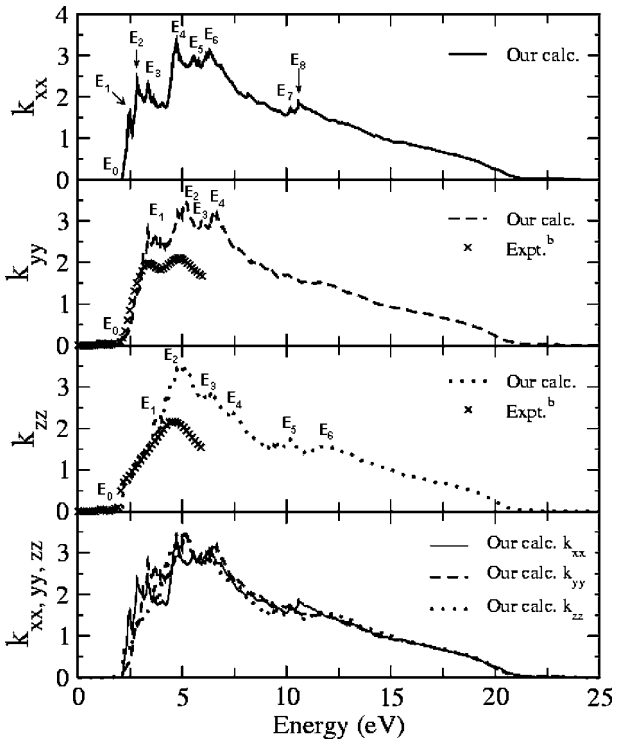

FIG. 16. Calculated and experimental imaginary part of the complex index of refraction. [b]Ref. 7.

p_y-Ge (Fig. 5) and a minor contribution of p_x, p_y-S valence states (Fig. 7), and it is in correspondence with the E_5 peak in ε_{2zz}. Both experimental results[47,48] start at almost the same energy (see E_0 in Table V) and show a peak that clearly corresponds to our E_2, but of less strength. Only one of the measured[48] dielectric functions presents a second peak (hardly seen in Fig. 13, see Table V), which we associate with our E_3. The experimental results also present a shoulder that might correspond to our calculated one, formed by E_5 and E_6. With regard to the [010] direction, our calculated ε_{yy} shows a similar aspect to that of ε_{xx} but with a less deep valley between the two principal peaks (E_1 and E_2). Theoretical and experimental curves are in good agreement, although the experimental curve corresponding to the ε_{xx} lacks the prominent peak E_4. We suggest that the problem lies on the experimental conditions, owing to the fact that there are technical difficulties in preparing samples cleaved in planes perpendicular to that of natural cleavage.[8,44,47,48] This implies the existence of an important source of error in any measurement for light polarized parallel to the direction of the crystal largest axes.

The three available experimental results shown in Fig. 13 have smaller amplitudes than the ones we calculated. Although none of them presents a structure of the strength of our E_2 peak in ε_{xx}, the curve of Ref. 47 shows a similar morphology. The result of Ref. 48 displays a broad shoulder in the range of energies corresponding to E_2. Concerning the y and z axis, experimental and theoretical results are also in excellent agreement, although none of the experimental measurements reaches the amplitudes corresponding to E_2 and E_3. It is to be noted, though, that the three experimental results disagree with each other in these aspects. Figure 7 shows that the morphology of p_z-Ge and p_z-S states is coherent with the resultant ε_{2zz}.

As to the coefficient of extinction (Fig. 16), even though there are no experimental results on k_{xx} to compare with, the notable peaks were labeled and quantitatively assessed in Table VI. As to the origin of the peaks, given the close relation to those of ε_2, it is expected to be the same. In k_{yy} the calculated shoulder E_1 and the peak E_2 clearly relate to the only experimental curves available,[7] while in k_{zz}, E_2 is 0.39 eV behind the experimental peak. Both calculated curves are in excellent agreement with the experimental ones, which range from 0 to 6 eV, except for some overestimation of amplitudes.

Figure 17 and Table VII show our calculated coefficient of absorption for each of the three axes, compared to measured absorptions at 92 K for the a and c axes (in our notation), performed by Elkorashy.[8] As to the morphology, all three absorptions start at the same energy, defining an isotropic energy gap E_0 of 1.12 eV. However, the three absorption edges grow at different rates, α_{zz} being the fastest (steepest) and α_{yy} the slowest (least steep). This is in favor of the idea of a band gap being located in the $\Gamma \rightarrow Z$ line of the BZ. In addition, a special feature of α_{yy} must be mentioned: it presents a steep growth followed by a flat, narrow shoulder that

TABLE VI. Relevant peaks of the coefficient of extinction. Energies are in eV.

	k_{xx}		k_{yy}		k_{zz}	
Peaks	Our calc.	Expt.	Our calc.	Expt.	Our calc.	Expt.
E_0	2.16		2.23	2.00[a]	1.98	2.00[a]
E_1	2.51		3.71	3.31[a]	3.85	
E_2	2.88		5.13	4.85[a]	4.95	4.56[a]
E_3	3.44		5.96		6.14	
E_4	4.70		6.58		7.44	
E_5	5.56				10.15	
E_6	6.30				11.96	
E_7	10.15					
E_8	11.67					

[a]Reference 7.

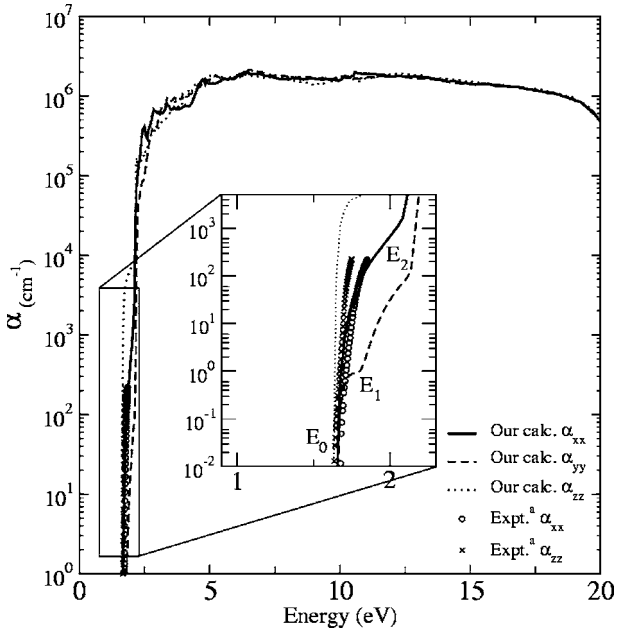

FIG. 17. Calculated and experimental coefficient of absorption. [a]Ref. 8.

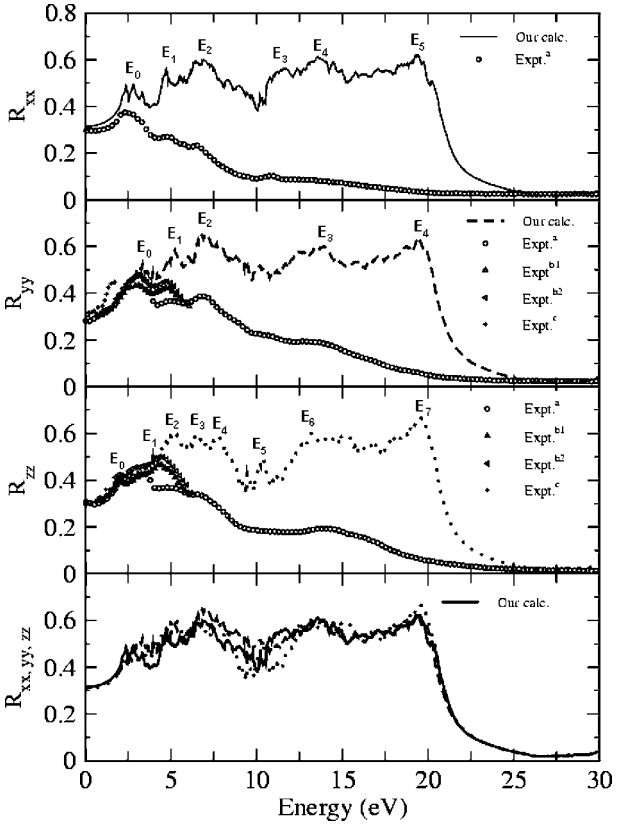

FIG. 18. Calculated and experimental coefficient of reflection. [a]Ref. 47, [b1]Ref. 7 (obtained with the Krammer-Kronig approximation), [b2]Ref. 7 (direct measurement), [c]Ref. 8.

ends in E_1, and a broader shoulder that goes from E_1 to E_2. These shoulders can be understood as the result of p_y-Ge and p_y-S contributions: Fig. 7 shows how this "shouldered" behavior occurs for the p_y states contribution, both in the valence and conduction bands (for Ge). The general behavior of our calculations is in clear agreement with Elkorashy's experimental result.[8]

With regard to reflectivity (Fig. 18 and Table VIII), a general look at our results shows that all three calculated reflectivities do not fall together with the experimental ones. Instead, they keep fluctuating about the value of 0.5, only to abruptly drop at about 19.00 eV. The calculated reflectivities obtain excellent agreement for $R(0)$ in the three directions. As to the detailed spectra, R_{xx} presents six prominent structures (E_0-E_5), four of which are in good correspondence as to the location in energy but not as to the amplitude, with the experimental results (E_0–E_3) of Ref. 47. For R_{yy} and R_{zz} there is good agreement among the experimental results up to about 4.00 and 3.00 eV, respectively. For greater energies only calculated and measured reflectivities of Eymard (Expt.^{b1} and Expt.^{b2} in Fig. 18, respectively), remain in mutual correspondence. It is worth noticing that the reflectivity and the absorption coefficient for the three axes, present the expected similar profile. Besides, in order to compare our results with those of Ref. 48, we present a detailed description of the reflectivity fine structure for the range 0–6.50 eV in Fig. 19 and Table IX. An excellent agreement was obtained, as can be seen in Table IX.

D. Final remarks

The material presents anisotropy in its three axes, a characteristic feature of GeS shown in the bottom graphic of Figs. 11–13, 16, and 18. When characterizing this material, it is evident that disagreements among experimental results and between theoretical and experimental results appear. Differences in amplitude might be a consequence of experimental conditions such as room temperature (it has been shown that the dielectric function of GeS falls with the increase of temperature[49]), finite thickness of the studied slab (which has been reported to be of importance in the reflective response

TABLE VII. Relevant peaks of the coefficient of absorption. Energies are in eV.

	α_{xx}		α_{yy}		α_{zz}	
Peaks	Our calc.	Expt.	Our calc.	Expt.	Our calc.	Expt.
E_0	1.66	1.67[a]	1.66		1.63	1.63[a]
E_1			1.80			
E_2			2.13			

[a]Reference 8.

TABLE VIII. Experimental and calculated reflectivity at zero energy and notable peaks. All values are in eV, except for $R(o)$ which are adimensional.

	R_{xx}		R_{yy}		R_{zz}	
$R(0)$/peaks	Our calc.	Expt.	Our calc.	Expt.	Our calc.	Expt.
$R(0)$	0.31	0.29[a]	0.28	0.28[a]	0.31	0.31
				0.32[c]		0.31[c]
E_0	2.72	2.50[a]	3.38	3.13[a]	1.94	2.03[a]
				3.13[b]		2.03[b]
				1.70[c]		
E_1	4.71	5.04[a]	5.20	5.07[a]	3.98	3.50[a]
				4.79[b]		3.50[b]
E_2	6.85	6.58[a]	6.90	6.92[a]	5.12	5.07[a]
						4.52[b]
E_3	11.55	10.88[a]	13.73		6.60	
E_4	13.62		19.57		7.67	
E_5	19.42				10.33	
E_6					13.33	
E_7					19.57	

[a]Reference 47.
[b]Reference 7 (calculated with the Kramers-Kronig approximation); Reference 7 (directly measured).
[c]Reference 8.

of the slabs utilized for the experiments[50]), and surface defects (especially in planes perpendicular to the cleavage plane[48]). The discrepancy with the results of Ref. 47 is most likely due to poor quality of the surface polishing, commented on by the authors themselves, rather than to inaccuracy of our calculations. In fact, it has been inferred from ellipsometry measurements that the contact of GeS with the air has major consequences on the optical properties of its surface. It is likely that an overlayer of amorphous germanium sulfide exists (possibly Ge_xS_{1-x}, which is 4:2 coordinated and satisfies the coordination of Ge and S better than the crystalline GeS).[51] Although the experimental measurements naturally provide smoother curves than the theoretical ones, and in this case lower amplitudes than the ones we computed, a good agreement and characterization have been clearly achieved by our calculations.

V. CONCLUSIONS

We have used an *ab initio* FP-LAPW method to determine the electronic structure and, in particular, the location and nature of the energy band gap of a GeS semiconductor. Also, from our calculated conduction band DOS, we have obtained very good agreement with the experimental core excitation spectra. We show that the spin-orbit interaction does not introduce significant changes in the description of the electronic structure of the material. Neither did we find important differences between the LDA and the GGA approximations. In addition, we show that the description of the material as a layered compound must include the effects of the hybridization of the *s-p* states at the edge of the valence band, in order to provide an appropriate description of the band structure.

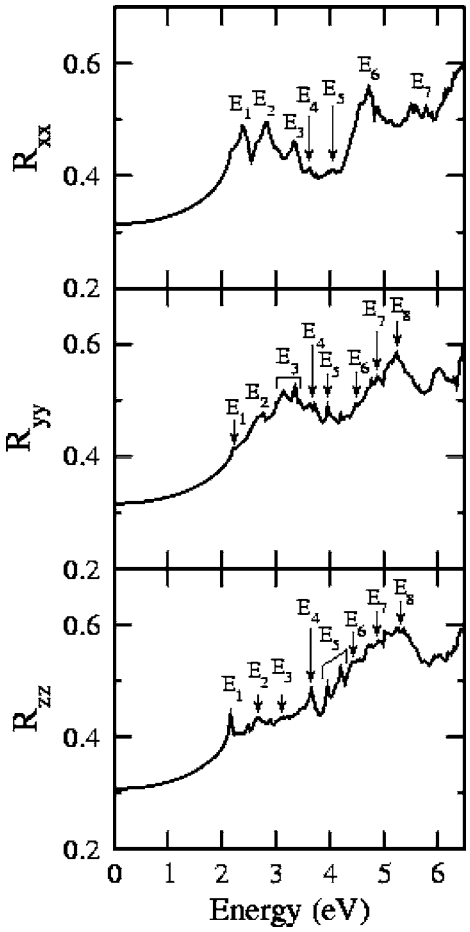

FIG. 19. Fine structure of our calculated coefficient of reflectivity. See Table IX.

TABLE IX. Fine structure critical-point energies up to 5 eV (modified Table II in Ref. 48, axes according to our notation). All values are in eV.

	Our calc. reflectivity peaks	Expt.[a]	Expt.[b]	Expt.[c]	Expt.[d]	Other calc.[e]
x axis ($\mathbf{E}\|a$ polarization)						
E_0					~1.65	
E_1	2.39	2.078(18)	2.2			
E_2	2.83	2.623(17)	2.5			
E_3	3.34	3.310(45)	3.3			
E_4	3.64	3.788(85)				
E_5	4.03	4.028(25)				
E_6	4.73	4.623(41)	4.7			
E_7	~5.70					
y axis ($\mathbf{E}\|b$ polarization)						
E_0				1.661		1.2
E_1	2.21	2.047(6)	2.1	2.15	~2.2	1.8
				2.52		~2.6
E_2	2.75	2.610(9)	2.7	2.63		~3.0
E_3	3.13	3.096(17)		2.98		~3.1
	3.38			3.28		~3.4
E_4	3.66	3.668(19)		3.45	3.3	~3.8
E_5	3.99	4.043(12)		4.15		~4.0
E_6	4.48	4.563(28)	5.0	4.50	4.5	~4.5
E_7	4.83	~4.95		4.9		~5.0
E_8	5.24					
z axis ($\mathbf{E}\|c$ polarization)						
E_0						
E_1	2.17	2.037(10)		1.588	~1.65	1.2
E_2	2.65	2.637(6)	2.0	2.034	~2.2	2.2–2.4
E_3	3.16	3.162(46)	2.8	2.642		2.5–2.7
E_4	3.67	3.628(17)				
E_5	3.97	4.031(13)	3.4	3.55	~3.5	3.2–3.6
	4.20			4.10		~4.2
				4.3	4.3	~4.4
E_6	~4.52	4.53(9)	4.9			~5.0
E_7	~4.80					
E_8	~5.20					

[a]Reference 48.
[b]Reference 47.
[c]Reference 52.
[d]Reference 7.
[e]Reference 13.

The behavior of these cationic s states is a characteristic of the IV-VI materials. Our calculations give multiple energy gaps that explain the diversity of the available experimental results. With this electronic structure we have also thoroughly computed and characterized the optical response of GeS, obtaining very good agreement with the available experimental data, although we found discrepancies in the reflectivities for energies higher than 5 eV corresponding to UV and x-ray incident light, since the experimental data of Ref. 47 give low and descending reflectivity curves for this region.

ACKNOWLEDGMENTS

The authors wish to thank Niels E. Christensen for very valuable discussions on this work. The authors acknowledge financial support from the Universidad Nacional de Entre Ríos (UNER), and the Consejo Nacional de Investigaciones Científicas y Técnicas (CONICET), Argentina.

*Electronic address: lmakinistian@ceride.gov.ar// eaa@intec.ceride.gov.ar

[1] Z. Shi, G. Xu, P. J. McCann, X. M. Fang, N. Dai, C. L. Felix, W. W. Bewley, I. Vurgaftman, and J. R. Meyer, Appl. Phys. Lett. **6**, 3688 (2000).
[2] T. Schwarzl, M. Böberl, W. Heiss, G. Springholz, J. Fürst, and H. Pascher, Proc. GMe Forum **2003**, 103 (2003).
[3] M. Böberl, W. Heiss, T. Schwarzl, K. Wiesauer, and G. Springholz, Appl. Phys. Lett. **82**, 4065 (2003).
[4] Th. Schwarzl, W. Heiß, G. Kocher-Oberlehner, and G. Springholz, Semicond. Sci. Technol. **14**, L11 (1999).
[5] R. B. Shalvoy, G. B. Fisher, and P. J. Stiles, Phys. Rev. B **15**, 2021 (1977).
[6] L.-M. Yu, A. Degiovanni, P. A. Thiry, J. Ghijsen, R. Caudano, and P. Lambin, Phys. Rev. B **47**, 16222 (1993).
[7] R. Eymard and A. Otto, Phys. Rev. B **16**, 1616 (1977).
[8] A. M. Elkorashy, J. Phys. C **21**, 2595 (1988); and references therein.
[9] J. D. Wiley, W. J. Buckel, and R. L. Schmidt, Phys. Rev. B **13**, 2489 (1976).
[10] H. R. Chandrasekhar, R. G. Humphreys, and M. Cardona, Phys. Rev. B **16**, 2981 (1977).
[11] M. Taniguchi, R. L. Johnson, J. Ghijsen, and M. Cardona, Phys. Rev. B **42**, 3634 (1990).
[12] H. C. Hsueh, M. C. Warren, H. Vass, G. J. Ackland, S. J. Clark, and J. Crain, Phys. Rev. B **53**, 14806 (1996).
[13] T. Grandke and L. Ley, Phys. Rev. B **16**, 832 (1977).
[14] F. M. Gashimzade, D. G. Guliev, D. A. Guseinova, and V. Y. Shteinshrayber, J. Phys.: Condens. Matter **4**, 1081 (1992).
[15] D. D. Koelling and G. O. Arbman, J. Phys. F: Met. Phys. **5**, 2041 (1975).
[16] O. K. Andersen, Phys. Rev. B **12**, 3060 (1975).
[17] O. Jepsen, J. Madsen, and O. K. Andersen, Phys. Rev. B **26**, 2790 (1982).
[18] M. Weinert, E. Wimmer, and A. J. Freeman, Phys. Rev. B **26**, 4571 (1982).
[19] H. J. F. Jansen and A. J. Freeman, Phys. Rev. B **30**, 561 (1984).
[20] L. F. Mattheiss and D. R. Hamann, Phys. Rev. B **33**, 823 (1986).
[21] S. Cottenier, *Density Functional Theory and the Family of (L)APW-Methods: A Step-by-Step Introduction* (Instituut voor Kern- en Stralingsfysica, K.U. Leuven, Belgium, 2002); http://www.wien2k.at/reg_user/textbooks
[22] L. H. Thomas, Proc. Cambridge Philos. Soc. **23**, 542 (1927).
[23] E. Fermi, Z. Phys. **48**, 73 (1928).
[24] P. Hohenberg and W. Kohn, Phys. Rev. **136**, B864 (1964).
[25] P. Blaha, K. Schwarz, and J. Luitz, WIEN code; P. Blaha, K. Schwarz, P. Sorantin, and S. B. Rickey, Comput. Phys. Commun. **59**, 399 (1990).
[26] W. Kohn and L. J. Sham, Phys. Rev. **140**, A1133 (1965).
[27] J. P. Perdew and Y. Wang, Phys. Rev. B **45**, 13244 (1992).
[28] J. P. Perdew, J. A. Chevary, S. H. Vosko, K. A. Jackson, M. R. Pederson, D. J. Singh, and C. Fiolhais, Phys. Rev. B **46**, 6671 (1992).
[29] J. P. Perdew, K. Burke, and M. Ernzerhof, Phys. Rev. Lett. **77**, 3865 (1996).
[30] J. P. Perdew, K. Burke, and M. Ernzerhof, Phys. Rev. Lett. **78**, 1396 (1997).
[31] J. P. Perdew, S. Kurth, A. Zupan, and P. Blaha, Phys. Rev. Lett. **82**, 2544 (1999).
[32] M. Lanoo, M. Schlüter, and L. J. Sham, Phys. Rev. B **32**, 3890 (1985).
[33] S. Wey and A. Zunger, Phys. Rev. B **55**, 13605 (1997).
[34] E. A. Albanesi, W. L. Lambrecht, and B. Segall, J. Vac. Sci. Technol. B **12**, 2470 (1994).
[35] R. Laskowski, N. E. Christensen, G. Santi, and C. Ambrosch-Draxl, Phys. Rev. B **72**, 035204 (2005).
[36] M. L. Cohen and J. R. Chelikowsky, *Electronic Structure and Optical Properties of Semiconductors*, 2nd ed., edited by M. Cardona, Springer Series in Solid State Sciences, Vol. 75 (Springer-Verlag, Berlin, 1989).
[37] Su-Hai Wei and A. Zunger, Phys. Rev. B **55**, 13605 (1997).
[38] E. A. Albanesi, C. M. I. Okoye, C. O. Rodriguez, E. L. Peltzery Blanca, and A. G. Petukhov, Phys. Rev. B **61**, 16589 (2000).
[39] L. Hedin, Phys. Rev. **139**, A796 (1965); L. Hedin and S. Lundquist in *Solid State Physics*, edited by H. Ehrenreich, F. Seitz, and D. Turnbull (Academic Press, New York, 1969), Vol. 23, p. 1.
[40] F. Araysetianwan and G. Gunnarson, Rep. Prog. Phys. **61**, 237 (1998).
[41] K. Hummer, C. Ambrosch-Draxl, G. Bussi, A. Ruini, M. J. Caldas, E. Molinari, R. Laskowski, and N. E. Christensen, Phys. Status Solidi B **242**, 1754 (2005).
[42] J. D. Wiley, A. Breitschwerdt, and E. Schönherr, Solid State Commun. **17**, 355 (1975).
[43] H. Haritonidis and D. S. Kyriakos, Semicond. Sci. Technol. **4**, 365 (1989).
[44] A. M. Elkorashy, J. Phys.: Condens. Matter **2**, 6195 (1990).
[45] P. E. Blöchl, O. Jepsen, and O. K. Andersen, Phys. Rev. B **49**, 16223 (1994).
[46] C. Ambrosch-Draxl and R. Abt, WIEN97, ICTP Lecture Notes (1998) (unpublished).
[47] J. D. Wiley, W. J. Buckel, W. Braun, G. W. Fehrenbach, F. J. Himpsel, and E. E. Koch, Phys. Rev. B **14**, 697 (1976); J. D. Wiley and G. W. Fehrenbach, *ibid.* **18**, 2963 (1978).
[48] S. Logothetidis, L. Viña, and M. Cardona, Phys. Rev. B **31**, 2180 (1985); and references therein.
[49] S. Logothetidis, P. Lautenschlager, and M. Cardona, Phys. Rev. B **33**, 1110 (1986).
[50] R. A. Süleymanov, S. Ellialtioğlou, and B. G. Akinoğlu, Phys. Rev. B **52**, 7806 (1995).
[51] S. Logothetidis and H. M. Polatoglou, Phys. Rev. B **36**, 7491 (1987).
[52] F. Lukeš, E. Schmidt, J. Humlíček, and P. Dub, Phys. Status Solidi B **122**, 675 (1984).